ACSNANO

www.acsnano.org

ARTICLE

Self-Rebound Cambered Triboelectric Nanogenerator Array for Self-Powered Sensing in Kinematic Analytics

Yutao Hao,[▽] Jing Wen,[▽] Xiaobo Gao,[▽] Ding Nan,* Juan Pan, Yuhan Yang, Baodong Chen,* and Zhong Lin Wang*

Cite This: https://doi.org/10.1021/acsnano.1c09096

Read Online

ACCESS | Metrics & More | Article Recommendations | Supporting Information

ABSTRACT: **In challenging and dangerous equestrian sports, kinematic analysis and injury prevention based on distributed, portable, and real-time sensing technology is particularly important. Here, we report a flexible self-rebound cambered triboelectric nanogenerator that addresses the concerns and shows its applications for self-powered sensing in kinematic analysis. Benefiting from simple and effective design, ordinary materials by means of self-rebound cambered structure evolved into a micro-biomechanical energy harvester with mechanical properties including over 3000 cycles durability and superior resiliency and stability. At a size of 4.52 cm^2, it could deliver a power density of 1.25 mW/m^2 under an external load resistance of 60 MΩ. A self-powered riding characteristic sensing system has been developed with fast response time of 16 ms, to provide real-time statistics data and fall prediction for both horsemen and coaches, to take traditional equestrian sports to a advanced state. This work not only can promote the development of triboelectric nanogenerators in micro-biomechanical energy harvesting, but also could expand the application range of the self-powered system to intelligent sport monitoring and assisting.**

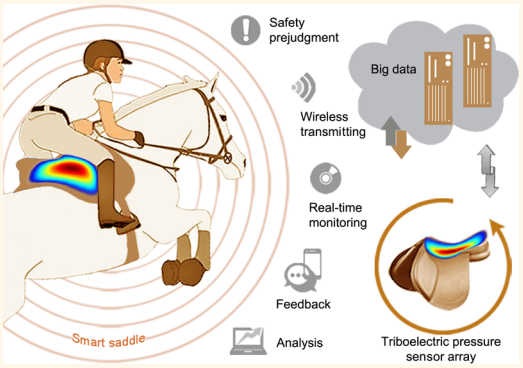

KEYWORDS: *self-powered sensing, triboelectric nanogenerator, self-rebound, safety prejudgment, kinematical analytics*

INTRODUCTION

With the rapid development of modern society and economy, in the era of he Internet of things (IoTs), big data collection and analysis based on distributed, portable, and real-time sensing technology is particularly important.[1] The sports field has also undergone revolutionary changes driven by technical advances and is reaching at a genuine digital, intelligent, and network age.[2,3] The contents include health data, training statistics, kinematic analytics, competition assistance and safety prediction, and information communication. Sports data is very important for athletes[4,5] and is becoming an indispensable means for winning competitions because it can not only collect important information such as sports time,[6] frequency,[7] and speed[8] but also intuitively know the state of the athletes through this information.[9] Usually, real-time data acquisition and monitoring of sport states relies on widely distributed sensors,[10,11] which are generally powered by various conventional batteries (including button cell, dry cell, and lithium-ion batteries).[12−14] But in certain circumstances, the existing technologies present difficulties achieving the goals, such as need for flexibility, portability, and durability and to avoid environmental pollution in the process of sports.[15−19] So, it is highly desirable to develop a maintenance-free and sustainable sensing technology that is matched to application requirements.[20,21]

The triboelectric nanogenerator (TENG) was invented by Z. L. Wang in 2012, based on coupling the effects of contact electrification and electrostatic induction,[22−27] has been developed into a pioneering technology for converting mechanical energy into electricity, and has the typical advantages of high efficiency, low cost, simple structure, lightweight, and diverse material options.[28−30] TENGs based on four basic working modes have been demonstrated and have comprehensive applications in mechanical energy harvesting (including wind, water wave, human activities,

Received: October 14, 2021
Accepted: January 4, 2022

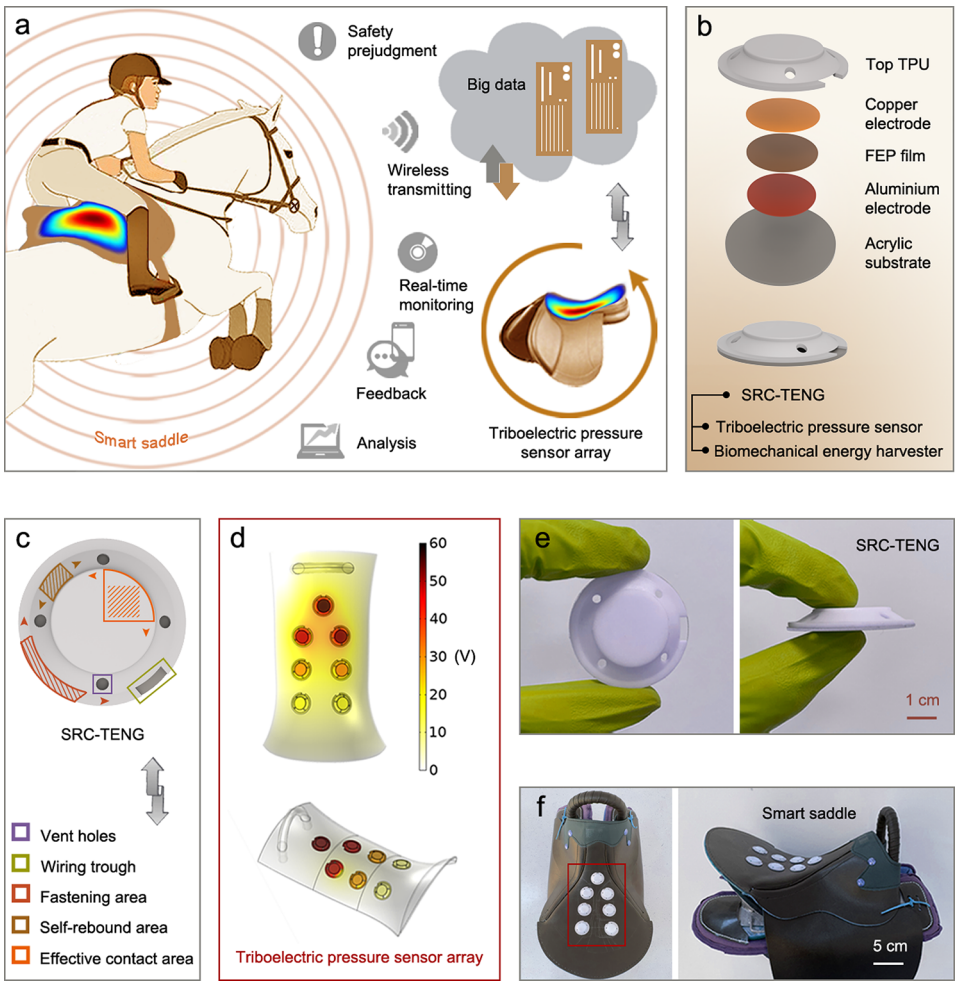

Figure 1. Structure design and schematic of SRC-TENG. (a) Overview of the smart saddle assembled on a horse to collect information and harvest energy. (b) Exploded view of structure design of the SRC-TENG. (c) Detailed structure information on the SRC-TENG. (d) Schematic illustration of SRC-TENG applied on the saddle and simulation diagram for the force distribution of the saddle using the COMSOL software. (e) Photographs of the SRC-TENG device. (f) Photograph of seven TENG units assembled on the saddle.

etc.), which can provide a sustainable power source for low-power electronics. In addition, TENGs can also operate as active sensors by directly converting mechanical stimuli (such as pressure, gentle touch, motion, or sound waves) to electrical signals, which is vital for developing maintenance-free self-powered sensing systems without an external power source.[31−33] Therefore, the promising TENGs can be a highly effective power supply technology for IoTs, sensor networks, robotics, man−machine interface, and artificial intelligence, where large amounts of distributed electronic devices should be applied. In the challenging and dangerous equestrian sports, kinematic analysis and injury prevention, which can possibly provide real-time statistical data and fall prediction for both horsemen and coaches, are particularly important. However, the mechanical properties and adaptability of conventional sensing technology are unsatisfactory for the intense sports.[34,35] Therefore, an effective solution that can improve the inadequacies of structure by rational design for fabricating a highly matched TENG, is superior for developing human adaptable, portable, and real-time self-powered sensing systems.

We propose a simple and effective design for fabricating a self-rebound cambered triboelectric nanogenerator (SRC-TENG) with excellent mechanical properties. With an effective contact area of 4.52 cm^2, the stable and durable SRC-TENG is capable of outputting a power density of 1.25 mW/m^2 under an external load resistance of 60 MΩ. An integrated SRC-TENG array can be utilized as both micro-biomechanical energy harvester and self-powered sensing system in kinematic analytics. Meanwhile, this device possesses other merits such as fast response speed (16 ms), small volume (diameter of 40 mm and height of 5 mm), low weight (4 g), and cost-effective production. By integration of a SRC-TENG array on a smart saddle, a self-powered riding characteristic sensing system, which can perform real-time data statistics and safety prediction with fast response time of 16 ms for both horsemen and coaches, was further developed. The successful demonstration of the SRC-TENG applied in a smart saddle can not only promote the development of TENGs in micro-biomechanical energy harvesting and sensing but also provide a possibility for self-powered systems in competitive sports, intelligent athletic facilities, and sport safety.

RESULTS AND DISCUSSION

Structural Design and Working Mechanism. As a micro-biomechanical energy harvester, the SRC-TENG has great potential for building self-powered sensing systems, which can be combined with a variety of existing sports

https://doi.org/10.1021/acsnano.1c09096
ACS Nano XXXX, XXX, XXX−XXX

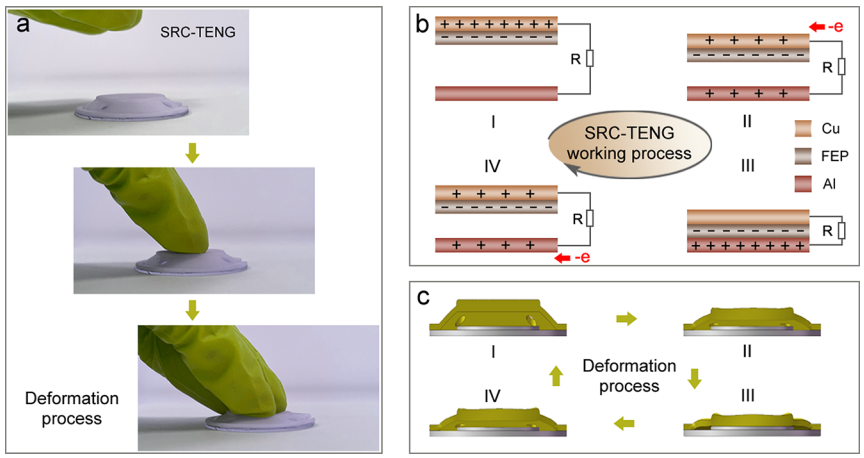

Figure 2. Working principle of the SRC-TENG. (a) Photographs illustrating the deformation process of the device. (b) Working mechanism of the SRC-TENG under vertical contact-separation mode. (c) 3D illustration of the working mechanisms of the TENG under external force.

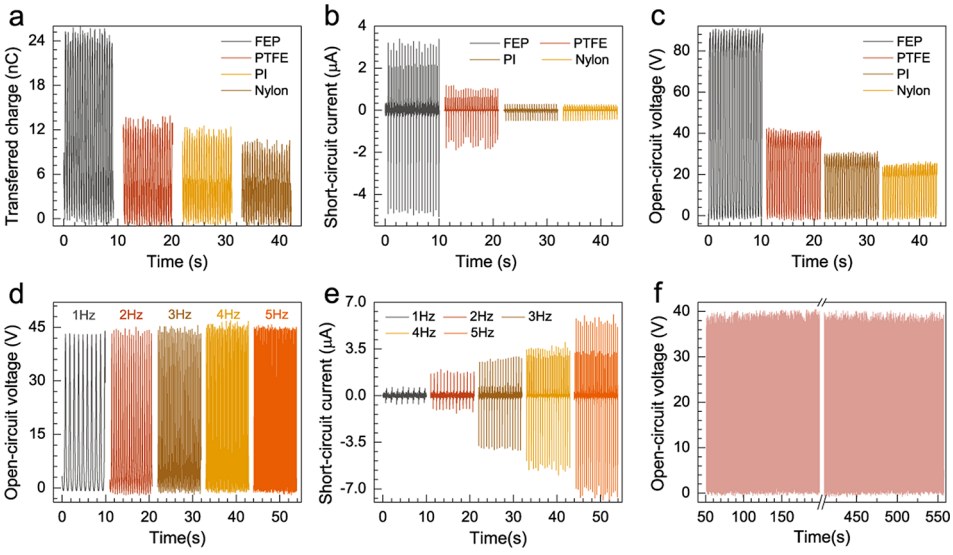

Figure 3. Electrical output performance of SRC-TENG. (a) Transferred charge, (b) short-circuit current, and (c) open-circuit voltage of SRC-TENG with various triboelectric layer materials. (d) Open-circuit voltage and (e) short-circuit current of the TENG with various pressing frequencies. (f) Mechanical durability characterization of the TENG unit with over 3000 continuous working cycles.

equipment such as the saddle. Figure 1a shows a conceptual schematic illustration of the smart saddle with some characteristics such as harvesting micro-biomechanical energy and a self-powered sensing system for kinematic analytics and safety prediction. The SRC-TENG array can be assembled on the surface of the saddle in order to accurately distinguish the pressure areas of the saddle and make better contact. An exploded view of device is shown in Figure 1b. A cambered rubber cover made of thermoplastic polyurethane (TPU) with 40 mm diameter acts as the top layer, having good mechanical properties and excellent flexibility. A copper electrode layer is attached to it, a fluorinated ethylene propylene (FEP, thickness of 80 μm) thin film was employed as the top triboelectric layer and stuck on the copper electrode, which has strong tendency to gain electrons. The substrate was fabricated of a thin acrylic plate (thickness of 1 mm) made with a laser cutter and integrated tightly with the cambered cover, so that it can well adapt to different equipment because of the adaptable rigidity. An Al film was attached to the acrylic substrate and was used both as another triboelectric layer and as an electrode. The structure design and detailed parameters of the device can be seen in Figure S1. The self-rebound cambered cover with characteristics of flat top and cambered sides is graphically illustrated in Figure 1c. The flat top can make sufficient contact between the two triboelectric layers, and the cambered sides can make the device recover from deformation quickly by itself in an extensive pressure range when the pressure is removed. The four vent holes around the cambered surface maintain the pressure balance of device. The overall design not only is simple in structure, easy to manufacture, and small in size, but also possesses excellent mechanical robustness to make the device more reliable and durable for long-term functioning in outdoor activities. The SRC-TENG has great potential for building a self-powered sensing system in sports equipment. Taking equestrian sports as an example, the SRC-TENG can be applied to fabricate a smart saddle. Due to the excellent structure, resulting in a response time of 16 ms, the resolution of SRC-TENG is at the same level as traditional small wired motion sensors, but it has advantages of lower energy consumption, lighter weight, and easy installation for a self-powered sensing and safety prediction system. As shown in the simulation diagram in Figure 1d, the SRC-TENG sensor array

https://doi.org/10.1021/acsnano.1c09096
ACS Nano XXXX, XXX, XXX−XXX

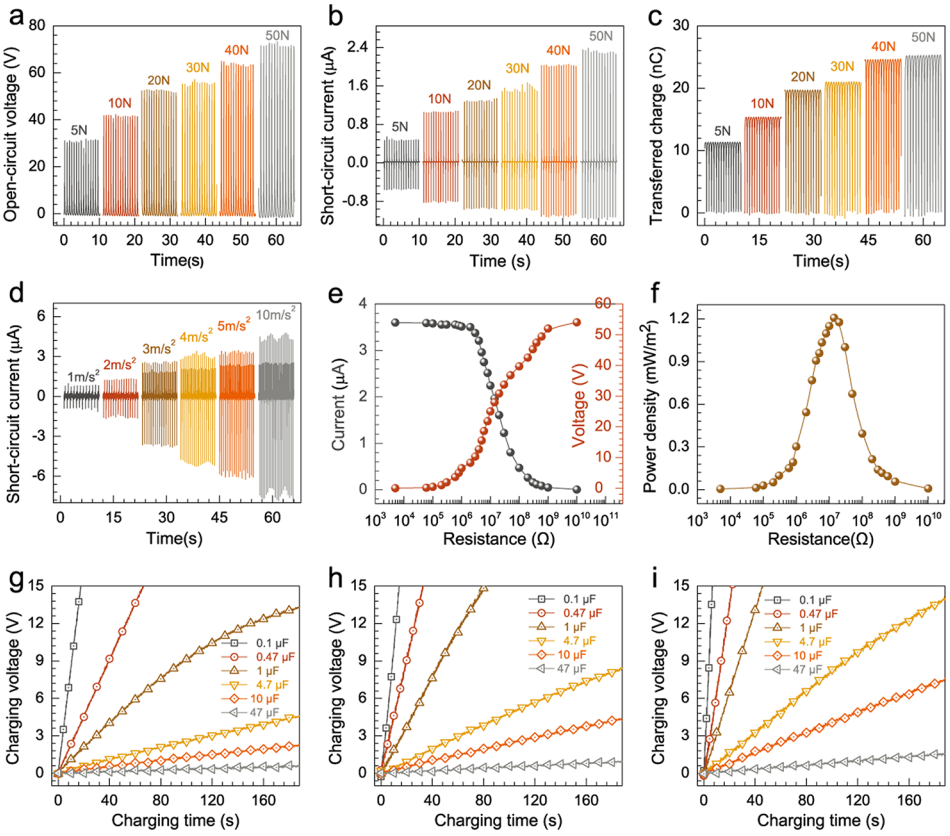

Figure 4. Electrical characterization of the TENG. (a) Transferred charge, (b) open-circuit voltage, and (c) short-circuit current of SRC-TENG with different applied forces. (d) Short-circuit current of SRC-TENG in different accelerations. (f) Peak power density and (e) measured output current and voltage on different external loading resistances. (g) Single unit, (h) three unit, and (i) five unit charging performance of the TENGs in different capacitors.

simulates the potential distribution according to the pressure when a person sits on the saddle; through this we can know the state of the rider immediately while riding, which is significant for sports equipment and training. Figure 1e presents photographs of the device at different angles and photographs of a saddle assembled with the SRC-TENG array on the surface are exhibited in Figure 1f.

The working mechanism of the SRC-TENG is based on coupling the effects of triboelectrification and electrostatic induction. When the SRC-TENG is pressed by an external force, the cambered cover will deform and bend. The photograph in Figure 2a presents the good compressibility of device. The energy generation process is shown in Figure 2b: When an external force is applied on the rubber cover, the two triboelectric layers are close to each other; due to the difference in triboelectric sequences, the same amount of charges with opposite polarities will be induced on the two electrodes, the electrification process occurs at the interface, a higher potential will be generated on the top electrode, and electrons will transfer from the aluminum electrode to the copper through the external circuit to counteract the potential difference, generating the current. When the two triboelectric layers fully contact each other, there is no current in the external circuit, because the charges on the surfaces of two layers are almost neutralized. During the separation period, the potential difference will increase, which causes the electrons to move toward the aluminum electrode from the copper electrode and generate current, until they separate a certain distance and the two triboelectric layers can reach electrical equilibrium. When the top cover is compressed again to get close to the substrate, the whole process will happen repeatedly, and an alternating current will be generated. The continuous operation of the SRC-TENG relies on compressive deformation and self-rebound of the shape. The 3D illustration is depicted in Figure 3c: during this motion cycle, the periodic alternating current will be generated with continuous contact separation movement. A theoretical study of a SRC-TENG has been carried out by means of finite element method in COMSOL software (Figure S2a). The result shows that the potential distribution changes with the distance between the two triboelectric layers, which is consistent with the previous argument. In addition, the typical electric signals of output voltage, current, and transferred charges in the motion processes are exhibited in Figure S2b–d.

Performance. The output performance of the SRC-TENG was demonstrated with a computer-controlled linear motor for all the tests, which can simulate various compression motions. We investigated the influence of the material of SRC-TENG at frequency of 2 Hz; several kinds of materials were used to fabricate SRC-TENGs. Figure 3a–c shows the output performance of the transferred charges (Q_{sc}), short-circuit current (I_{sc}), and open-circuit voltage (V_{oc}) with different materials (FEP, polytetrafluoroethylene (PTFE), polyimide (PI), and nylon) when other experimental conditions remain the same. The experiment proves that output performance is related to the divergent surface electron affinity: FEP is a more tribonegative material and has higher affinity to electrons, whereas nylon is a more tribopositive material. It can be

https://doi.org/10.1021/acsnano.1c09096
ACS Nano XXXX, XXX, XXX–XXX

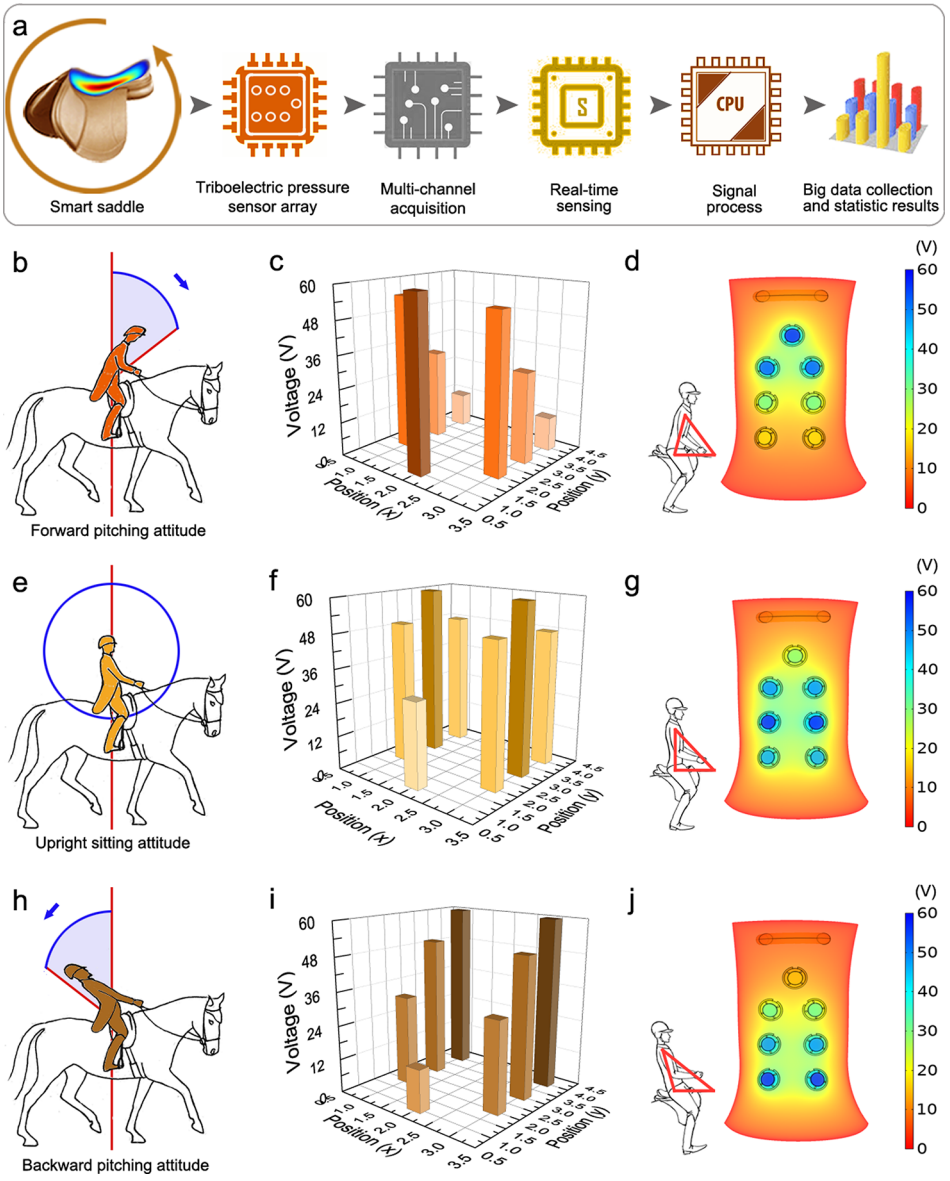

Figure 5. Self-powered riding characteristic sensing system for real-time statistical data and kinematic analysis. (a) Schematic diagram of smart saddle involved in a riding pitch attitude detection system. A pressing signal can be converted into a visual statistical result. (b) Forward pitching attitude illustration of athlete on the horse. (c) Output voltage from seven channels when the pressing position is on front part of the saddle. (d) Simulation diagram of the potential distribution on smart saddle under forward pitching attitude by using COMSOL software. (e) Upright pitching attitude illustration of athlete on the horse. (f) Output voltage from seven channels, when the pressing position is in the middle part of the saddle. (g) Simulation diagram of the potential distribution on the smart saddle with upright pitching attitude. (h) Backward pitching attitude illustration of athlete on the horse. (i) Corresponding reconstructed results in pressure sensory matrix. (j) Simulation diagram of the potential distribution on smart saddle under backward pitching attitude.

concluded that the FEP film is the optimal choice compared to the other materials. A TENG is greatly affected by the environment. In order to verify the accuracy of the experiment, we utilized the same material to repeat the experiment in the same environment to study the authenticity. The electrical output performance of the SRC-TENG is shown in Figure S3; there is no significant change in output performance, which can also prove the stability of the device. The performance of the SRC-TENG with different riding frequency was also studied. The V_{oc} and the I_{sc} with the riding frequency of the device are shown in Figure 3d,e. When the contact separation distance is 15 mm, under the different frequencies (1 to 5 Hz), the result shows that the voltage is constant around 45 V. Meanwhile, the current rose from 0.8 μA at 1 Hz to 4 μA at 5 Hz with the increasing frequency, which implies that a higher frequency is beneficial to produce a higher performance of I_{sc}, but it will not influence V_{oc}. The reason is the Q_{sc} values are constant under the different frequencies, whereas the number of contacts between two layers increase with the increasing operation frequency; therefore, higher frequency results in a higher transfer rate of charges, resulting in a higher I_{sc}. Subsequently, we investigated the long-term reliability and stability of the SRC-TENG. As shown in Figure 3f, after operation over 3000 cycles, the V_{oc} shows no obvious degradation, which fully demonstrates the significant robustness and durability of device and proves the stability and practicability of the SRC-TENG in terms of micro-biomechanical energy harvesting and motion monitoring.

https://doi.org/10.1021/acsnano.1c09096
ACS Nano XXXX, XXX, XXX−XXX

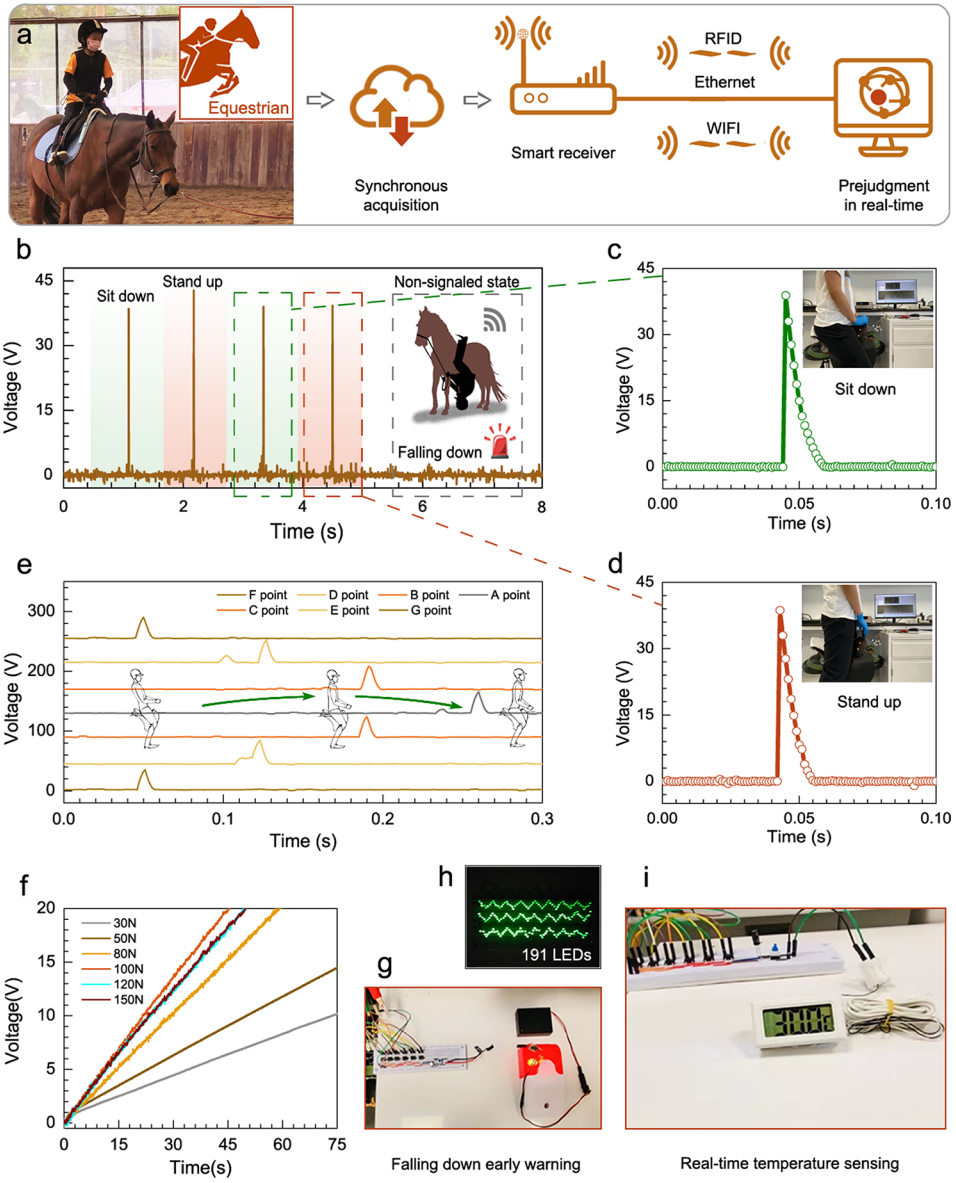

Figure 6. Application of the ARC-TENG based smart saddle for safety prediction and micro-biomechanical energy harvest. (a) Schematic illustration and photographs of the application scenarios of TENG sensors for safety prediction and the associated transmission equipment. (b) Motion state monitoring signals of smart saddle in different conditions. (c) Sit down signal and (e) stand up signal during the riding state. (d) Real-time measurement of the seven sensors from forward pitching attitude to backward pitching attitude. (f) Charging performance of the TENG unit in different applied force. (g) Working state of the alarm receiving a warning signal from the transmitter. (h) Photograph of nearly 200 LEDs lit up by the TENG array during the riding process. (j) Photograph of an electronic thermometer driven by a TENG array charged capacitor during the riding process.

Meanwhile, we also investigated the influence on output performance of SRC-TENG from different external applied forces. A force gauge was used to measure the external applied force, and the device was operated under a frequency of 2 Hz and 15 mm contact distance. When the initial external applied force is 10 N, the voltage output is 40 V (Figure 4a); as the applied force increases, the output voltage also increases, and when the external applied force increases from 5 to 50 N, the I_{sc} also increased from 0.5 to 2.4 μA (Figure 4b). Figure 4c shows the increasing transferred charges as the external force rises. This result is expected because the two triboelectric layers get a better contact with the increasing external applied force, which means a large effective contact area and therefore a higher electrical output performance. Figure 4d shows the I_{sc} of the SRC-TENG at different accelerations (from 1 to 10 m s^{-2}); the I_{sc} of the SRC-TENG increases from 1.2 μA at 1 m s^{-2} to 6.5 μA at 10 m s^{-2} because the I_{sc} is determined by both charge density and charge-transfer rate, and when the acceleration increases, the charge transfer rate increases. In Figure 4e, we show the output performance of the SRC-TENG with different external resistance. When the resistance increased from 10^4 Ω to 10^{10} Ω, the V_{oc} increased from 0 to 55 V, but the I_{sc} decrease incrementally due to the ohmic loss. With the increasing resistance, the instantaneous power increased steadily at first and then tended to decrease when it reached the peak value. The corresponding power density is 1.25 mW/m^2 with external loading resistance of 60 MΩ (Figure 4f). Moreover, to further evaluate the performance of

https://doi.org/10.1021/acsnano.1c09096
ACS Nano XXXX, XXX, XXX−XXX

the charging ability, we selected different amounts of SRC-TENG assembled on the saddle, and the linear motor was used to simulate the riding movement to charge the capacitor. The output voltage signal was collected by the Keithley 6514. The assembly diagram of the smart saddle and a photograph of operation under test system is shown in Figure S4. As shown in Figure 4g–i, under external forces of 30 N and frequency of 2 Hz, as the number of SRC-TENG units increases, the charging time becomes faster. Therefore, we can conclude that more devices assembled on a saddle result in acceleration of charging speed. Moreover, in the SRC-TENG array, because of the different contact times of the devices on the saddle, the motion phase consistency is hard to reach; as a result, the output current of the SRC-TENG array is not five times that of the single unit.

Demonstration. The SRC-TENG can be also used as a pressure triboelectric sensor to establish a wireless riding characteristic sensing system as depicted in Figure 5a; the circuit design of the system and simulation diagram of the TENG array when human sits on saddle is shown in Figure S5. By placement of seven SRC-TENG units on the saddle from front to back as sensing points, which can detect the applied pressure, when a person sits on the saddle in various postures, different pulse signals will be generated on the sensors, and each sensor connects with the multichannel acquisition. Based on the collection and analysis of different voltages at the seven points, the distribution of pressure can be calculated, and we can get information about riding pitch attitude through terminal equipment by utilizing some electronic modules. Figure 5b–d shows the pressure sensory matrix and simulation diagram of a person sitting on the saddle with forward pitching attitude; the three high output voltage points (around 50 V) can be detected at the front of saddle, but other points show V_{oc} under 40 V, which is significantly lower than the front part. Therefore, we can know that the person is in a forward pitching attitude from the signal, and the corresponding simulation diagram obtains a sensitive and potential distribution image which can also confirm this result. Based on this identification strategy, a variety of riding pitch attitudes can be also monitored. When a pressure contact position test was conducted at the middle of the saddle (Figure 5e–g), a higher output voltage can be detected in the middle position of saddle, about 58 V, and the voltage of the sensors in other positions are significantly lower than those in the middle. It can be also inferred from the simulation diagram in Figure 5g: a higher potential appears in the middle part, which means that the middle part has more applied pressure than the surrounding part, so it would be judged that the athlete is in an upright pitching attitude. When the voltage of the sensor array at the end of the saddle is higher, decreasing from back to front, it is recognized as a backward pitching attitude. In order to further verify its utility for big data analysis for equestrian sports, the signal and simulation diagrams of other three different riding pitch attitudes are shown in Figure S6, and the signal appeared simultaneously when a person made a corresponding posture. By big data collection and analysis of the statistical result, the athlete's exercise habit data can be gained to assist their training and improve competition tactics. The self-powered pitching attitude monitoring system based on SRC-TENG provides a possibility for the manufacture smart equipment for equestrian training.

With the rapid development of equestrian sports, people are paying more and more attention to safety issues while riding. The major danger comes from the direct injury due to falling from the horse and the inability to be found in time after falling. In order to improve the safety of athletes in the process of riding, a self-powered fall warning system was built based on the SRC-TENG. The SRC-TENG array was assembled on the surface of the saddle, which is used as sensor for the warning system and sends out an alarm after collecting and processing data. The progress is shown in Figure 6a. A signal will be generated when a person sits on the; through the method of multichannel data acquisition, the real-time voltage signals of every sensor could be detected at the same time, and then the transmitter will send the processed signal to the terminal equipment in real time. Figure 6b shows a riding signal for a period of time; during this process, before falling, the sensor continuously puts out a stable signal; the rising and sitting voltage signals are shown in Figure 6c,d. However, when the smart saddle no longer puts out the signal, we can judge based on the signals that the athlete may have fallen from the horse. The corresponding signal will be sent out through the transmitter and activate the alarm; the equivalent circuits of the warning system and the photograph of the alarm in working state are shown in Figure S7a,b. In order to fulfill the potential of the riding characteristic sensing system, the signal is collected from SRC-TENG through multichannel method and statistical analysis of the data is performed, enabling the output to reflect dynamically the riding pitch attitude and pressure distribution on the smart saddle. Figure 6e shows the posture change process of the athlete; from backward posture to forward posture the voltage signal appears successively in the corresponding channels over time, which means that the sensor can also be used for continuous monitoring of riding pitch attitude. To further investigate the viability of the SRC-TENG to power the electronics by harvesting micro-biomechanical energy, the relationship between external applied force and the voltage across the capacitor was measured. We utilized a vertical linear motor acts as the external drive, which provides a variety of applied forces in a vertical direction. The charging time of the capacitor under different applied forces is shown in Figure 6f. As the applied force increases, the charging speed also becomes faster, which means a larger force can lead o better contact, thereby reducing the charging time. It is clearly seen that more than 200 commercial LEDs were lit by the smart saddle (Figure 6h and Movie S1). The SRC-TENG array charges the capacitor and through the rectifier bridge can power the electronics intermittently. When the capacitor was charged for 20 min, it could activate a thermometer once, with power consumption of approximately 36 μJ, as shown in Figure 6g–i. Movies S2 and S3 demonstrate the ability to collect micro-biomechanical energy under applied force from a linear motor to power the transmitter and thermometer. The corresponding photograph of working status, specific connection method, and components of the circuit are shown in Figure S7c–f. This experiment demonstrates the long-term potential of SRC-TENG for being widely used in intelligent devices and sensors.

CONCLUSIONS

We proposed a flexible and self-rebound cambered triboelectric nanogenerator (SRC-TENG) for self-powered sensing in kinematic analysis and safety prediction. Benefiting from simple and effective design, ordinary materials by means of self-rebound cambered structure evolved into a high-performance micro-biomechanical energy harvester with excellent

https://doi.org/10.1021/acsnano.1c09096
ACS Nano XXXX, XXX, XXX–XXX

mechanical properties including over 3000 cycle durability and superior resiliency and stability. With a size of 4.52 cm^2 per unit, it could deliver a power density of 1.25 mW/m^2 under an external load resistance of 60 MΩ. By integration of a SRC-TENG array on a smart saddle, a self-powered riding characteristic sensing system was further developed with fast response time of 16 ms, which can sense the micro-biomechanical energy generated by equestrian sports and monitor the riding state by its own sensitive self-rebound structure to provide real-time statistical data and fall detection for both horsemen and coaches. Taking these compelling advantages into account, the SRC-TENG has great application prospects in the fields of micro-biomechanical energy harvesting and analysis of sport mechanics. It provides significant guidance for the development of self-powered sensing technology toward distributed, portable, and real-time analysis in the next stage.

EXPERIMENTAL SECTION

Fabrication of the SRC-TENG. The SRC-TENG in this work consisted of two main parts: The arc cover is made by a 3D printing process, using the TPU material with hardness of 65A, the wall thickness is 1 mm, and the overall height is 5 mm. Four air vents were evenly distributed on the side. A layer of copper thin film (24 mm in diameter) serving as an electrode was placed on the rubber film. Subsequently, a FEP film of the same size was attached on the copper electrode as the triboelectric layer. An acrylic board (thickness of 1 mm) was cut with laser cutter to 40 mm in diameter as the substrate. An aluminum film was attached on the surface of the acrylic sheet, then the top cover was glued onto the acrylic sheet.

Characterization and Measurement. The electric output of the SRC-TENG was tested with a programmable electrometer (Keithley Instruments model 6514). A vertical linear motor (Linmot E1100) was applied to drive the SRC-TENG with different parameters.

ASSOCIATED CONTENT

Supporting Information

The Supporting Information is available free of charge at https://pubs.acs.org/doi/10.1021/acsnano.1c09096.

Structure design of the SRC-TENG, potential distribution and typical electrical output performance of the SRC-TENG, electrical output performance of the SRC-TENG with different triboelectric materials, photograph of smart saddle based on the SRC-TENGs and testing system, circuit design and illustration of SRC-TENG array arrangement on the saddle, self-powered riding characteristic sensing system for real-time statistical data and kinematic analysis, circuit diagram and photographs of the system and each component (PDF)

Movie S1, lighting LEDs by human applied external force to SRC-TENG (MP4)

Movie S2, demonstration of the SRC-TENGs to power a transmitter (MP4)

Movie S3, demonstration of the SRC-TENGs to power a thermometer (MP4)

AUTHOR INFORMATION

Corresponding Authors

Ding Nan − *College of Chemistry and Chemical Engineering, Inner Mongolia University, Hohhot 010021, P. R. China; School of Materials Science and Engineering, Inner Mongolia University of Technology, Hohhot 010051, P. R. China*; Email: nd@imu.edu.cn

Baodong Chen − *Beijing Institute of Nanoenergy and Nanosystems, Chinese Academy of Sciences, Beijing 101400, P. R. China; School of Nanoscience and Technology, University of Chinese Academy of Sciences, Beijing 100049, P. R. China; Institute of Applied Nanotechnology, Jiaxing, Zhejiang 314031, P. R. China*; orcid.org/0000-0002-4647-0089; Email: chenbaodong@binn.cas.cn

Zhong Lin Wang − *Beijing Institute of Nanoenergy and Nanosystems, Chinese Academy of Sciences, Beijing 101400, P. R. China; School of Nanoscience and Technology, University of Chinese Academy of Sciences, Beijing 100049, P. R. China; School of Materials Science and Engineering, Georgia Institute of Technology, Atlanta, Georgia 30332-0245, United States*; orcid.org/0000-0002-5530-0380; Email: zlwang@gatech.edu

Authors

Yutao Hao − *College of Chemistry and Chemical Engineering, Inner Mongolia University, Hohhot 010021, P. R. China; School of Materials Science and Engineering, Inner Mongolia University of Technology, Hohhot 010051, P. R. China; Institute of Applied Nanotechnology, Jiaxing, Zhejiang 314031, P. R. China*

Jing Wen − *Beijing Institute of Nanoenergy and Nanosystems, Chinese Academy of Sciences, Beijing 101400, P. R. China; School of Nanoscience and Technology, University of Chinese Academy of Sciences, Beijing 100049, P. R. China*

Xiaobo Gao − *School of Materials Science and Engineering, Inner Mongolia University of Technology, Hohhot 010051, P. R. China; Institute of Applied Nanotechnology, Jiaxing, Zhejiang 314031, P. R. China*

Juan Pan − *College of Chemistry and Chemical Engineering, Inner Mongolia University, Hohhot 010021, P. R. China; Institute of Applied Nanotechnology, Jiaxing, Zhejiang 314031, P. R. China*

Yuhan Yang − *School of Materials Science and Engineering, Inner Mongolia University of Technology, Hohhot 010051, P. R. China; Institute of Applied Nanotechnology, Jiaxing, Zhejiang 314031, P. R. China*

Complete contact information is available at: https://pubs.acs.org/10.1021/acsnano.1c09096

Author Contributions

[▽]Y. H., J. W., and X. G. contributed equally to this work. D.N., B.C., Z.L.W., and Y.H. conceived the project and designed the experiments. Y.H., J.W., and X.G. contributed to sample preparation. Y.H. and J.W. performed the experiments. X.G., J.P., and Y.Y., contributed to data analysis. All authors discussed the results and commented on the manuscript. Y.H., D.N., B.C., and Z.L.W. wrote the manuscript with input from all authors.

Notes

The authors declare no competing financial interest.

ACKNOWLEDGMENTS

The authors acknowledge the support from Natural Science Foundation of Beijing Municipality (2192062), supported by National Natural Science Foundation of China (51502147, 51702018, 51502147, and 11704032). The research was sponsored by the National Key R & D Project from Minister of Science and Technology (2016YFA0202704), the Beijing Municipal Science and Technology Commission

(Z181100003818016 and Y3993113DF), Inner Mongolia scientific and technological achievements transformation project (CGZH2018132), and Inner Mongolia autonomous region major science and technology project (2020ZD0024).

REFERENCES

(1) Ye, C.; Dong, K.; An, J.; Yi, J.; Peng, X.; Ning, C.; Wang, Z. L. A Triboelectric–Electromagnetic Hybrid Nanogenerator with Broadband Working Range for Wind Energy Harvesting and a Self-Powered Wind Speed Sensor. *ACS Energy Letters* **2021**, 1443–1452.
(2) Luo, J.; Gao, W.; Wang, Z. L. The Triboelectric Nanogenerator as an Innovative Technology toward Intelligent Sports. *Adv. Mater.* **2021**, *33*, No. e2004178.
(3) Umek, A.; Zhang, Y.; Tomazic, S.; Kos, A. Suitability of Strain Gage Sensors for Integration into Smart Sport Equipment: A Golf Club Example. *Sensors (Basel)* **2017**, *17*, 916.
(4) Ahmadi, A.; Mitchell, E.; Richter, C.; Destelle, F.; Gowing, M.; O'Connor, N. E.; Moran, K. Toward Automatic Activity Classification and Movement Assessment during a Sports Training Session. *IEEE Internet of Things Journal* **2015**, *2*, 23–32.
(5) Lin, Z.; Wu, Z.; Zhang, B.; Wang, Y.-C.; Guo, H.; Liu, G.; Chen, C.; Chen, Y.; Yang, J.; Wang, Z. L. A Triboelectric Nanogenerator-Based Smart Insole for Multifunctional Gait Monitoring. *Advanced Materials Technologies* **2019**, *4*, 1800360.
(6) Wang, H.; Wang, J.; Xia, X.; Guan, D.; Zi, Y. Multifunctional Self-Powered Switch toward Delay-Characteristic Sensors. *ACS Appl. Mater. Interfaces* **2020**, *12*, 22873–22880.
(7) Walker, A. M.; Applegate, C.; Pfau, T.; Sparkes, E. L.; Wilson, A. M.; Witte, T. H. The Kinematics and Kinetics of Riding a Racehorse: A Quantitative Comparison of a Training Simulator and Real Horses. *J. Biomech* **2016**, *49*, 3368–3374.
(8) Jin, L.; Zhang, S. L.; Xu, S.; Guo, H.; Yang, W.; Wang, Z. L. Free-Fixed Rotational Triboelectric Nanogenerator for Self-Powered Real-Time Wheel Monitoring. *Advanced Materials Technologies* **2021**, *6*, 2000918.
(9) Chen, X.; Wu, Y.; Shao, J.; Jiang, T.; Yu, A.; Xu, L.; Wang, Z. L. On-Skin Triboelectric Nanogenerator and Self-Powered Sensor with Ultrathin Thickness and High Stretchability. *Small* **2017**, *13*, 1702929.
(10) Deng, C.; Tang, W.; Liu, L.; Chen, B.; Li, M.; Wang, Z. L. Self-Powered Insole Plantar Pressure Mapping System. *Adv. Funct. Mater.* **2018**, *28*, 1801606.
(11) Chen, B.; Tang, W.; Jiang, T.; Zhu, L.; Chen, X.; He, C.; Xu, L.; Guo, H.; Lin, P.; Li, D.; Shao, J.; Wang, Z. L. Three-Dimensional Ultraflexible Triboelectric Nanogenerator Made by 3D Printing. *Nano Energy* **2018**, *45*, 380–389.
(12) Schwartz, G.; Tee, B. C.; Mei, J.; Appleton, A. L.; Kim, D. H.; Wang, H.; Bao, Z. Flexible Polymer Transistors with High Pressure Sensitivity for Application in Electronic Skin and Health Monitoring. *Nat. Commun.* **2013**, *4*, 1859.
(13) Wu, Z.; Tang, J.; Zhang, X.; Yu, Z. An Energy Harvesting Bracelet. *Appl. Phys. Lett.* **2017**, *111*, 013903.
(14) Yamada, T.; Hayamizu, Y.; Yamamoto, Y.; Yomogida, Y.; Izadi-Najafabadi, A.; Futaba, D. N.; Hata, K. A Stretchable Carbon Nanotube Strain Sensor for Human-Motion Detection. *Nat. Nanotechnol* **2011**, *6*, 296–301.
(15) Zhang, C.; Liu, L.; Zhou, L.; Yin, X.; Wei, X.; Hu, Y.; Liu, Y.; Chen, S.; Wang, J.; Wang, Z. L. Self-Powered Sensor for Quantifying Ocean Surface Water Waves Based on Triboelectric Nanogenerator. *ACS Nano* **2020**, *14*, 7092–7100.
(16) Stone, E.; Skubic, M. Evaluation of an Inexpensive Depth Camera for In-Home Gait Assessment. *Journal of Ambient Intelligence and Smart Environments* **2011**, *3*, 349–361.
(17) Zhang, B.; Wu, Z.; Lin, Z.; Guo, H.; Chun, F.; Yang, W.; Wang, Z. L. All-In-One 3D Acceleration Sensor Based on Coded Liquid–Metal Triboelectric Nanogenerator for Vehicle Restraint System. *Mater. Today* **2021**, *43*, 37–44.
(18) Roy, A. L.; Sarkar, H.; Dutta, A.; Bhattacharyya, T. K. A High Precision SOI MEMS–CMOS ± 4g Piezoresistive Accelerometer. *Sensors and Actuators A: Physical* **2014**, *210*, 77–85.
(19) Wang, Z. L. Entropy Theory of Distributed Energy for Internet of Things. *Nano Energy* **2019**, *58*, 669–672.
(20) Xia, K.; Zhu, Z.; Zhang, H.; Du, C.; Xu, Z.; Wang, R. Painting a High-Output Triboelectric Nanogenerator on Paper for Harvesting Energy from Human Body Motion. *Nano Energy* **2018**, *50*, 571–580.
(21) Xia, K.; Wu, D.; Fu, J.; Xu, Z. A Pulse Controllable Voltage Source Based on Triboelectric Nanogenerator. *Nano Energy* **2020**, *77*, 105112.
(22) Wang, Z. L. Triboelectric Nanogenerator (TENG)—Sparking an Energy and Sensor Revolution. *Adv. Energy Mater.* **2020**, *10*, 2000137.
(23) Liu, W.; Wang, Z.; Wang, G.; Liu, G.; Chen, J.; Pu, X.; Xi, Y.; Wang, X.; Guo, H.; Hu, C.; Wang, Z. L. Integrated Charge Excitation Triboelectric Nanogenerator. *Nat. Commun.* **2019**, *10*, 1426.
(24) Liu, Y.; Liu, W.; Wang, Z.; He, W.; Tang, Q.; Xi, Y.; Wang, X.; Guo, H.; Hu, C. Quantifying Contact Status and the Air-Breakdown Model of Charge-Excitation Triboelectric Nanogenerators to Maximize Charge Density. *Nat. Commun.* **2020**, *11*, 1599.
(25) Lin, Z.; Zhang, B.; Guo, H.; Wu, Z.; Zou, H.; Yang, J.; Wang, Z. L. Super-Robust and Frequency-Multiplied Triboelectric Nanogenerator for Efficient Harvesting Water and Wind Energy. *Nano Energy* **2019**, *64*, 103908.
(26) Xu, C.; Wang, A. C.; Zou, H.; Zhang, B.; Zhang, C.; Zi, Y.; Pan, L.; Wang, P.; Feng, P.; Lin, Z.; Wang, Z. L. Raising the Working Temperature of a Triboelectric Nanogenerator by Quenching Down Electron Thermionic Emission in Contact-Electrification. *Adv. Mater.* **2018**, *30*, No. e1803968.
(27) Pu, X.; Hu, W.; Wang, Z. L. Toward Wearable Self-Charging Power Systems: The Integration of Energy-Harvesting and Storage Devices. *Small* **2018**, *14*, 1702817.
(28) Jin, L.; Chen, J.; Zhang, B.; Deng, W.; Zhang, L.; Zhang, H.; Huang, X.; Zhu, M.; Yang, W.; Wang, Z. L. Self-Powered Safety Helmet Based on Hybridized Nanogenerator for Emergency. *ACS Nano* **2016**, *10*, 7874–7881.
(29) Xu, S.; Zhang, L.; Ding, W.; Guo, H.; Wang, X.; Wang, Z. L. Self-Doubled-Rectification of Triboelectric Nanogenerator. *Nano Energy* **2019**, *66*, 104165.
(30) Zhang, S. L.; Jiang, Q.; Wu, Z.; Ding, W.; Zhang, L.; Alshareef, H. N.; Wang, Z. L. Energy Harvesting-Storage Bracelet Incorporating Electrochemical Microsupercapacitors Self-Charged from a Single Hand Gesture. *Adv. Energy Mater.* **2019**, *9*, 1900152.
(31) Wu, Z.; Ding, W.; Dai, Y.; Dong, K.; Wu, C.; Zhang, L.; Lin, Z.; Cheng, J.; Wang, Z. L. Self-Powered Multifunctional Motion Sensor Enabled by Magnetic-Regulated Triboelectric Nanogenerator. *ACS Nano* **2018**, *12*, 5726–5733.
(32) Li, R.; Wei, X.; Xu, J.; Chen, J.; Li, B.; Wu, Z.; Wang, Z. L. Smart Wearable Sensors Based on Triboelectric Nanogenerator for Personal Healthcare Monitoring. *Micromachines (Basel)* **2021**, *12*, 352.
(33) Xiao, T. X.; Liang, X.; Jiang, T.; Xu, L.; Shao, J. J.; Nie, J. H.; Bai, Y.; Zhong, W.; Wang, Z. L. Spherical Triboelectric Nanogenerators Based on Spring-Assisted Multilayered Structure for Efficient Water Wave Energy Harvesting. *Adv. Funct. Mater.* **2018**, *28*, 1802634.
(34) Xia, K.; Wu, D.; Fu, J.; Hoque, N. A.; Ye, Y.; Xu, Z. A High-Output Triboelectric Nanogenerator Based on Nickel–Copper Bimetallic Hydroxide Nanowrinkles for Self-Powered Wearable Electronics. *Journal of Materials Chemistry A* **2020**, *8*, 25995–26003.
(35) Xia, K.; Fu, J.; Xu, Z. Multiple-Frequency High-Output Triboelectric Nanogenerator Based on a Water Balloon for All-Weather Water Wave Energy Harvesting. *Adv. Energy Mater.* **2020**, *10*, 2000426.

https://doi.org/10.1021/acsnano.1c09096
ACS Nano XXXX, XXX, XXX–XXX